ORIGINAL PAPER

The effects of micro- and meso-scale characteristics on the mechanical properties of coal-bearing sandstone

Qiangling Yao [1,2] · Liqiang Yu [1,2] · Xuehua Li [1,2] · Kai Yan [1,2] · Qiang Xu [1,2] · Weinan Wang [1,2] · Chuanjin Tang [1,2]

Abstract

Studying the effects of the micro- and meso-scale characteristics of coal-bearing sandstone on its mechanical properties can provide basic data and accumulated experience for the development of technology for the in situ testing of the strength of rock masses. In this paper, the micro- and meso-structures, mineral composition, and elemental contents of 16 kinds of sandstone from three coal mines were studied through X-ray diffraction and polarizing microscope analysis. The stress–strain evolutional characteristics of different sandstone samples were obtained through uniaxial compression, tension, and shear tests under acoustic emission monitoring, and the effect of various micro- and meso-characteristics on the mechanical properties and failure characteristics of the sandstones was investigated. The results show that the strength, elastic modulus, cohesion, and friction coefficient all increase with increasing quartz content and degree of particle contact, and decrease with increasing plagioclase and clay mineral content, especially kaolinite content. The failure mode of sandstone samples is mainly shear failure during uniaxial compression, the larger the particles and the lower the quartz content, the higher the RA value generated near the peak, indicating that more tensile failure occurs. Furthermore, the strength damage model and damage constitutive model are established by acoustic emission measurement data. These results could provide useful reference for the development of intelligent systems for the in situ testing of the mechanical properties of coal and rock masses.

Keywords Coal-bearing sandstone · Micro- and meso-characteristics · Mechanical properties · Damage model

Introduction

Coal accounts for 58% of China's energy consumption, and it is expected that China's energy consumption will still be dominated by coal (more than 50%) in the next 10 years (Yao et al. 2020). The development of rock mechanics theory has laid a foundation for the development of the coal mining industry (Meng and Su 2006). In the process of coal mining, the understanding of the physical and mechanical properties of coal and rock masses profoundly affects the safety of mining operations. At present, the evaluation of the strength and stability of coal-

rock masses mostly depends on laboratory tests and in situ tests. The latter is widely used because it can overcome the disadvantages of disturbance and size effects of samples in laboratory tests (Ma et al. 2012). In situ test methods for coal-rock mass strength include large-scale compression shear tests (Hudson and Harrison 2009), impact hammer method (Peng et al. 2007; Zhao and Wu 2009), acoustic detection method (Bai et al. 2007), drilling measurement method (Wang and Yu 1998), and borehole penetration method (Kang and Wang 2007; Kang and Lin 2001). The relatively advanced ones are portable in situ test systems developed by Yao et al. (2019), which can realize large-scale and rapid test of the strength, elastic modulus, cohesion, internal friction angle, and ground stress of coal and rock mass on site. However, the current technologies lack the ability of systematic in situ automatic identification and intelligent decision-making, and cannot adapt to the complex geological conditions with many types of coal and rock masses and various mineral compositions. Laboratory measurements of the strength of coal and rock masses at the micro- and meso-scale can provide a foundation, which can quantitatively investigate the relationship between

---

Responsible Editor: Domenico M. Doronzo

✉ Liqiang Yu
  yuliqiangcumt@163.com

1 State Key Laboratory of Coal Resource and Safe Mining, China University of Mining & Technology, Xuzhou 221116, China

2 School of Mines, China University of Mining & Technology, Xuzhou 221116, China

the strength of coal and rock masses and the surface particle distribution and meso-structure characteristics of such rock masses. Therefore, it is of great importance to study the influence of micro- and meso-scale characteristics on the mechanical properties of rock to improve technologies for the in situ automatic determination of the mechanical properties of coal-rock masses and improving the safety of coal mine production.

Due to differences in diagenesis and stress environments, the micro- and meso-characteristics of minerals can vary significantly during the process of rock formation (Meng et al. 2002). Many scholars have extensively studied the mechanical properties of rocks based on their micro- and meso-characteristics. It is found that mineral composition, microfracture, porosity, particle size, particle shape, and intercrystalline structure are the most important factors affecting rock mechanical properties (Räisänen 2004; Lindqvist et al. 2007; Johansson 2011). Ersoy and Waller (1995) quantitatively analyzed the influence of fabric coefficient on rock mechanical properties by using imaging analysis system and found that the mechanical properties of the rocks depended on the rock fabric. Based on existing theory, Li and Michel (2003) developed and generalized a more suitable formula for the estimation of the uniaxial strength and porosity of materials, and applied this formula to materials, such as rock, ceramics, and concrete. Additionally, the researchers noted that the effect of fabric characteristics on the rock's mechanical properties is stronger than the effect of mineral composition. Charles (2002) and Homand et al. (2004) studied the effect of the mineral composition of clay rocks on the rocks' compressive strength and investigated the strength change and deformation characteristics of the clay rocks under saturated and partially saturated conditions. Thury and Bossart (1999) investigated the effect of micro-crystalline particles in clay rock on the rock's mechanical strength. Meng et al. (2000, 2002) established a quantitative relationship between rock microstructure and macro-mechanical properties. From the above researches, the internal factors that cause differences in the macro-mechanical properties of rocks were the mineral composition of rock-forming materials; the size, shape, and distribution characteristics of diagenetic particles; and microfissures (Zhao et al. 2013).

Research on the influence of micro- and meso-scale characteristics on rock mechanical properties always involves the investigation of rock damage mechanisms. Fonseka and Krajcinovic (1981) first introduced the concept of rock damage mechanisms. Starting with an analysis of the stress and strain states of brittle rock, they carried out relevant experimental research and theoretical derivation about rock damage mechanisms. Lemaitre (1996) established a constitutive relationship by representing complex rock-fissure parameters. Arbabi and Sahimi (1993) and Sahimi and Arbabi (1993) developed a theory regarding the weakest chain strength of materials. Barbero et al. (2005) stated that the general behavioral model of self-

healing materials included irreversible processes and healing processes, and proposed a constitutive model of damage healing based on continuous thermodynamics. Darabi et al. (2012) established a damage-healing model based on the concepts of Kachanov effective configuration and effective stress space. The experimental research and theoretical analysis of the above researchers has promoted the development of research into rock damage mechanics and laid a foundation for the application of such research in engineering.

In conclusion, many factors affect the mechanical properties of rock. Besides the effects of external factors, such as the stress conditions, environment, and characteristics of a sedimentary rock, the rock structure and composition also play a decisive role in determining the rock's mechanical properties (Meng et al. 2002). At present, there are few comparative studies on the mechanical properties of rocks in specific areas from the micro- and meso-scale. Therefore, research on the factors which affect the mechanical properties of rocks (especially for specific regions) is of great significance for the in situ testing of the strength of coal-rock masses.

Experimental scheme

Experimental materials and sample preparation

In this study, coal-bearing sandstones from the Jining No. 3 coal mine, the Dongqu coal mine, and the Xinqiao coal mine (mine locations shown in Fig. 1) were taken as research samples. The Jining No. 3 coal mine is located in Rencheng District, Jining City, Shandong Province (Fig. 1). The mine's strata mainly include the following: Middle and Lower Ordovician rocks, the Upper Carboniferous Benxi Formation, the Carboniferous Permian Taiyuan Formation, the Lower Permian Shanxi Formation, the Middle Permian
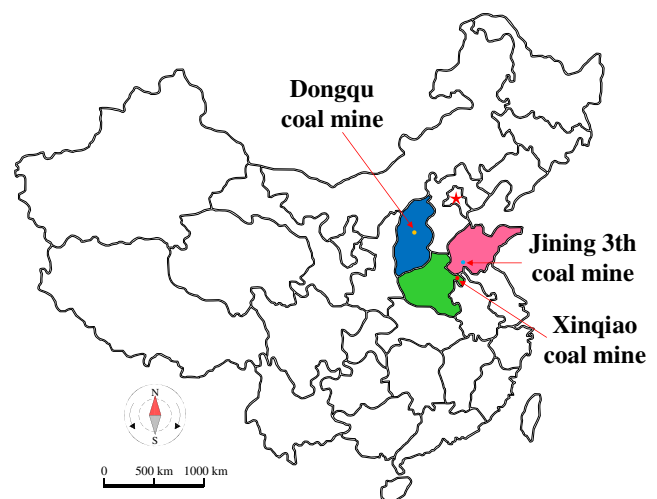

Fig. 1 Locations of the coal mines from which the sandstone samples were obtained

Table 1 Classification of sandstone samples

Mining area	Group number	Rock name	Description of rock structure	Sampling position
Jining No. 3 coal mine	A1-1-1	Argillaceous fine-grained feldspar quartz greywacke	1	Belt haulage roadway (roof; working face no. 7304)
	A2-1-1	Medium-fine lithic-debris feldspar sandstone I	2	
	A3-1-1	Medium-fine lithic-debris feldspar sandstone II	2	
	A4-1-1	Fine-medium lithic-debris feldspar sandstone	2	
	A5-1-1	Medium-fine lithic-debris feldspar sandstone III	2	
Dongqu coal mine	B1-1-1	Calcareous fine-grained lithic-debris quartz sandstone	3	Maintenance roadway (roof; 860 m a.s.l.)
	B2-1-1	Medium-grained lithic-debris sandstone	4	
	B3-1-1	Fine-grained lithic-debris greywacke I	4	
	B4-1-1	Medium-fine lithic-debris greywacke I	5	
	B5-1-1	Fine-grained lithic-debris greywacke II	6	Track transport roadway (roof; working face no. 24808)
	B6-1-1	Medium-fine lithic-debris greywacke II	5	
	B7-1-1	Coarse-grained lithic-debris greywacke I	6	
	B8-1-1	Coarse-grained lithic-debris greywacke II	7	
Xinqiao coal mine	C1-1-1	Coarse medium-grained feldspar lithic-debris I sandstone I	7	Main haulage roadway (roof)
	C2-1-1	Coarse medium-grained feldspar lithic-debris II sandstone II	8	
	C3-1-1	Coarse medium-grained feldspar lithic-debris III sandstone III	8	

Note: 1: argillaceous fine sandy structure, sub-edge-angular, particles sit in a miscellaneous matrix, base-type cementation, miscellaneous-matrix support; 2: medium-fine sandy structure, sub-edge-angular and sub-circular mineral shape, main particle contact is line contact, a small amount of point contact and concave–convex contact, porosity cementation, particle support; 3: fine sandy structure, edge-angular mineral shape, main particle contact is non-contact or point contact, a small amount of line contact, matrix-type cementation, miscellaneous-matrix support; 4: fine sandy structure, sub-edge-angular mineral shape, main particle contact is line contact, a small amount of concave–convex contact, porosity cementation, particle support; 5: fine sandy structure, sub-edge-angular and sub-circular mineral shape, main particle contact is non-contact, a small amount of point contact, matrix-type cementation, miscellaneous-matrix support; 6: medium-fine sandy structure, sub-edge-angular and sub-circular mineral shape, main particle contact is non-contact, a small amount of point contact, matrix-type cementation, miscellaneous-matrix support; 7: coarse sandy structure, sub-edge-angular and sub-circular mineral shape, main particle contact is non-contact or point contact, a small amount of line contact, matrix-type cementation, miscellaneous-matrix support; 8: coarse- to medium-grained sandy structure, sub-edge-angular, main particle contact is point contact, a small amount of line contact, porosity cementation, particle support

Lower Shihezi Formation and Upper Shihe Formation, the Upper Jurassic Mengyin Formation, and Quaternary rocks (Song et al. 2016a; Song et al. 2016b). The Dongqu coal mine is located to the southeast of Gujiao City, Shanxi Province (Fig. 1). The mine's strata are Cambrian, Ordovician, Carboniferous, Permian, Triassic, Neogene, and Quaternary in age (Su 2016; Zhou et al. 2017). The Xinqiao coal mine is located to the southwest of Yongcheng City, Henan Province (Fig. 1). The mine's strata are Cambrian, Ordovician, Carboniferous, Permian, Triassic, Tertiary, and Quaternary in age (Feng 2012; Xue 2012). The sandstone samples used in this study are from coal-bearing strata of the Lower Permian Shanxi Formation.

A total of 144 rock samples, representing 16 different types of sandstone, were selected, and the sedimentary rock classification scheme in the book *Sedimentary Petrology* by Zhang (1990) was adopted to classify them, as shown in Table 1.

In accordance with the requirements of the Test Specifications of the International Society of Rock Mechanics (Muralha et al. 2014) and Test Rules for the Physical and Mechanical Properties of Rocks (Ministry of Land and Resources of the PRC 2015), the original sandstone samples were respectively prepared into 48 cylinders with $\Phi50 \times 100$ mm, 48 cylinders with $\Phi50 \times 25$ mm, and into 48 cubes with a side length of 50 mm, for uniaxial compressive strength (σ_c), tensile strength, and shear strength tests respectively. The samples were grouped and numbered based on their lithological characteristics and source mine (Table 1). The letters A, B, and C indicate that the sample was obtained from the Jining No. 3 coal mine, Dongqu coal mine, and Xinqiao coal mine, respectively. The first number after the letter represents the type of sandstone, the second number represents the type of mechanical experiment, and the third number is the sample number. For example, sample A1-1-1 represents the first sample of argillaceous fine-grained feldspar quartz greywacke from the Jining No. 3 coal mine for uniaxial compression test. Additionally, the samples were crushed to allow X-ray diffraction analysis, while petrographic thin sections were prepared from each sample to facilitate polarizing microscope observation (Fig. 2).

Fig. 2 Thin sections (**a**) and hand specimens (**b**) of the analyzed sandstones

(a)   (b)
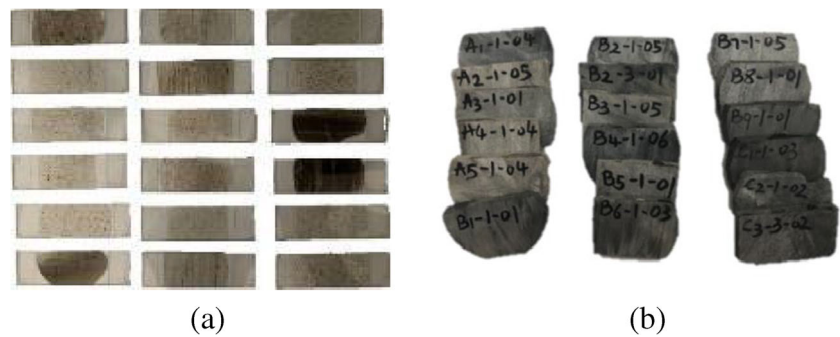
Experimental equipment and methods

According to the requirements of the Test Rules for the Physical and Mechanical Properties of Rocks (Ministry of Land and Resources of the PRC 2015) and the requirements for X-ray diffraction analysis, the rock samples were dried using a 101-2 air-blowing drier (Shanghai Instrument Factory, Shanghai, China). The drying temperature was set to 105 °C and the drying duration was 12 h. X-ray diffraction analysis was conducted on powdered rock samples using an X'Pert PRO X-ray diffractometer (PANalytical B.V., Almelo, Netherlands) in order to determine the mineral content of the rock samples. Microscopic analysis was performed on the rock thin sections using an XP-300 transmission digital polarizing microscope (Shanghai Tianxing, Shanghai, China) in order to obtain information about the micro- and meso-characteristics of the mineral composition, internal particle shape, particle arrangement, cementation, etc.

Uniaxial compressional, tensional, and shear tests were performed on the rock samples using a CMT5305 electronic universal testing system controlled by a micro-computer servo control system (Shenzhen SANS, Shenzhen, China). Uniaxial compression tests were conducted on the cylindrical samples with $\Phi 50 \times 100$ mm, uniaxial tension tests were conducted on the cylindrical samples with $\Phi 50 \times 25$ mm, and uniaxial shear tests were performed on the cubic rock samples. The loading rate was 0.5 mm/min under displacement loading. In the process of compressional failure of the rock samples, a TS3890N static resistance strain indicator (Beijing Zhongxi, Beijing, China) was used to record the axial strain of the rock samples, while a PCI-II AE system (PAC) was used to monitor the acoustic emission signals. The test system is shown in Fig. 3.

## Analysis of micro- and meso-characteristics of sandstone

X-ray diffraction analysis and polarizing microscope observation were carried out for the 16 different types of sandstone in order to determine their mineral

composition and mass fraction. The results are given in Table 2. Although 16 rock types were studied, due to the limitation of article length and similar analytical methods, only the results for argillaceous fine-grained feldspar quartz greywacke are presented. The results of the X-ray diffraction and polarizing microscope analysis of this rock sample are shown in Fig. 4.

From the polarizing microscope images, it can be seen that the argillaceous fine-grained feldspar quartz greywacke is gray in color, has a dominantly fine-grained sandy structure, and that its miscellaneous matrix has a mostly argillaceous structure. The content of lithic-debris (mainly including quartz debris, rock debris, and plagioclase debris) is about 56%, and the content of miscellaneous matrix is about 44%. The debris sits in an argillaceous miscellaneous matrix, and forms the support of this matrix and the matrix-type cementation. Most of this debris is sub-edge-angular; however, some is edge-angular. The results of the X-ray diffraction analysis show that the main minerals in the argillaceous fine-grained feldspar quartz greywacke sample (A1-1-1) are quartz, potassium feldspar, plagioclase, calcite, pyrite, illite, and kaolinite. Among these, quartz is dominant, accounting for 46.8% of the minerals, the potassium feldspar content is 2.0%, and the plagioclase content is 7.6%, while other clay minerals account for 43.6% of the minerals.

As shown in Table 1, the particle contact can be divided into four types: non-contact, point contact, line contact, and concave–convex contact. With increasing particle size, the particle-contact ratio decreases and the contact-type transitions from concave–convex contact or line contact to point contact or non-contact. As shown in Table 2, the selected sandstone is mainly composed of quartz, feldspar, and clay minerals. In all of the sandstones from the Jining No. 3 coal mine (mine A), the main minerals are fine-grained quartz, potassium feldspar, and plagioclase, and the contents of siderite, ankerite, and calcite are close to 0. In all of the sandstones from the Dongqu coal mine (mine B), the main minerals are medium- to fine-grained quartz and plagioclase; the contents of siderite, ankerite, and

Fig. 3 Schematic showing the testing system used for the analysis of rock mechanical parameters and acoustic emissions (AEs). 1: master control computer; 2: strain meter; 3: resistance strain gauge; 4: data transmission line; 5: wire; 6: preamplifier
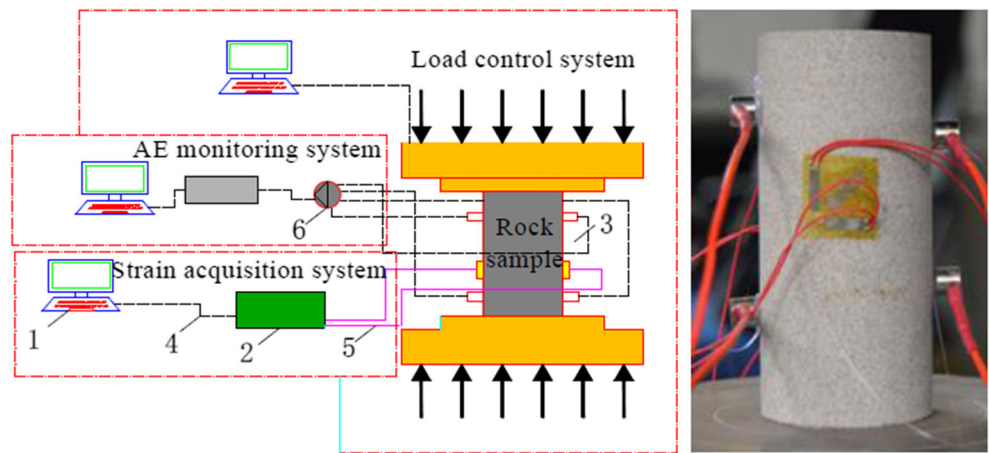
calcite are around 10%; and almost no potassium feld-spar is present. In the Xinqiao coal mine (mine C), the main type of sandstone is lithic-debris greywacke with a relatively coarse grain size. These rocks contain quartz, plagioclase, siderite, calcite, pyrite, and clays; however, they do not contain potassium feldspar or ankerite. The main clay minerals in the rock samples from the three mines are illite, smectite, kaolinite, and chlorite, the first two of which occur in mixed layers, and the clay min-eral contents of different types of sandstone are differ-ent. This analysis of sandstone composition lays a foun-dation for future analysis of the effects of clay minerals on the mechanical properties of rocks.

Study of the effects of micro- and meso-scale characteristics on the strength of sandstones

Mechanical properties and fissure characteristics of sandstones under uniaxial compression

Figure 5 shows the experimentally derived stress–strain curves for different types of sandstone from the three different mines under uniaxial compression, Table 3 shows the me-chanical properties of these rock samples. Sandstones in mine A have uniaxial compressive strengths of 18.47–58.34 MPa, elastic modulus of 1.18–2.19 GPa, and Poisson's ratios of 0.16–0.44; sandstones in mine B have uniaxial compressive

Table 2 Whole-rock mineral contents (in vol. %) of different types of sandstone

Group number	Total rock mineral content								Relative clay mineral content				
	Q	K-spar	Pl	Sid	Ank	Cal	Py	Clays	I	Kao	Chl	Formation	
												S/I	S%
A1-1-1	46.8	2.0	7.6	0.0	0.0	0.7	0.2	42.7	20	80	0	0	-
A2-1-1	37.5	22.3	17.4	0.0	0.0	0.4	0.1	22.3	24	34	21	21	15
A3-1-1	42.0	13.2	17.0	0.0	0.0	0.0	0.0	27.8	25	68	6	0	-
A4-1-1	38.7	18.7	19.0	0.0	0.0	0.8	0.1	22.6	27	37	24	12	12
A5-1-1	34.8	11.0	17.2	1.6	0.0	0.0	0.0	35.5	18	39	7	35	32
B1-1-1	49.2	0.0	7.4	1.9	0.0	0.0	0.1	41.5	68	12	3	18	12
B2-1-1	40.3	0.0	0.0	4.4	8.7	8.9	0.0	37.8	32	9	2	57	15
B3-1-1	46.5	0.0	0.0	1.5	1.3	0.0	0.1	50.6	96	1	2	0	-
B4-1-1	57.3	0.0	1.8	0.6	0.8	6.7	0.0	32.8	58	24	4	14	8
B5-1-1	44.3	0.0	4.0	0.7	0.0	1.6	0.0	49.4	63	5	1	31	8
B6-1-1	40.2	0.0	10.8	1.0	0.0	0.0	0.0	47.9	79	8	2	11	10
B7-1-1	44.2	0.0	3.2	4.1	0.0	3.8	0.0	44.8	82	7	2	9	9
B8-1-1	39.4	0.0	12.9	0.0	0.0	0.0	0.0	47.8	83	0	0	17	8
C1-1-1	35.4	0.0	6.7	4.5	0.0	0.0	1.3	52.1	58	28	4	11	9
C2-1-1	55.8	0.0	21.0	0.0	0.0	0.3	0.0	22.8	18	21	25	36	28
C3-1-1	63.8	0.0	18.7	1.8	0.0	0.0	0.0	15.7	70	0	0	29	8

Q, quartz; *K-spar*, potassium feldspar; *Pl*, plagioclase; *Sid*, siderite; *Ank*, ankerite; *Cal*, calcite; *Pv*, pyrite; *Clays*, clays; *I*, illite; *Kao*, kaolinite; *Chl*, chlorite; *Formation*, illite/smectite formation; *I*, illite; *S*, smectite

Fig. 4 Polarizing microscope images (**a** and **b**) and the X-ray diffraction spectrum (**c**) of argillaceous fine-grained feldspar quartz greywacke

(a)

(b)

(c)
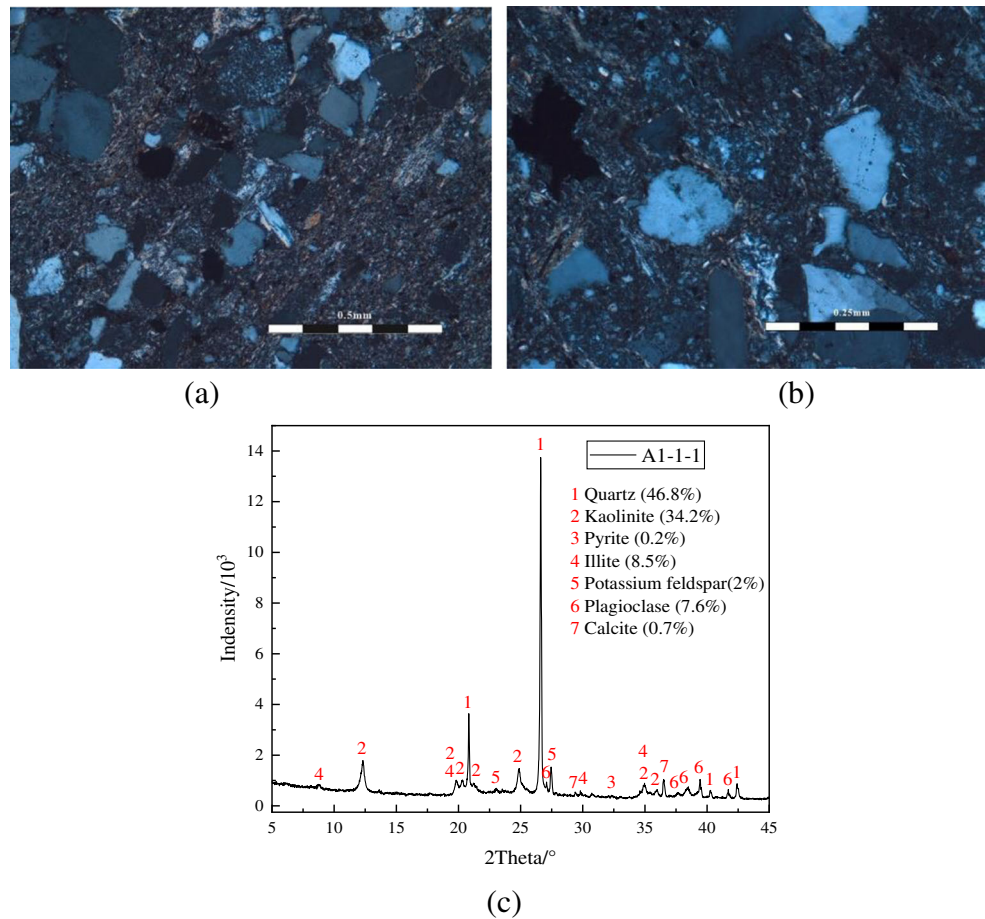
strengths of 26.81–82.83 MPa, elastic modulus of 1.27–2.62 GPa, and Poisson's ratios of 0.12–0.26; and sandstones in mine C have uniaxial compressive strengths of 26.87–82.08 MPa, elastic modulus of 1.31–2.67 GPa, and Poisson's ratios of 0.25–0.30. As shown in Fig. 5, different types of rocks show different deformation and failure characteristics under uniaxial compression. The pre-peak-stress deformation of samples in mine B is almost linearly elastic, showing obvious brittle failure characteristics. These rocks showed no precursory signals before failure; however, a loud noise and flying debris were produced when the rock samples were destroyed. As lithology changes, the uniaxial compressive strength of samples in mine A shows a decreasing trend, while their Poisson's ratio shows an increasing trend. The stress–strain curve for samples in mine C, especially sample C3-1-1 shows a serrated shape and an obvious stress drop during the fissure growth stage, which indicates that structural failure occurred before the sample had reached peak stress.

The cracks generated during brittle rock failure mainly consist of two kinds of crack: tensile cracks and shear cracks. The generation of different types of cracks generates different kinds of AE waveforms (Grosse and Ohtsu 2018). For example, the AEs generated by tensile fissures have shorter wavelengths, and the AE waveform has a shorter rising time and a higher frequency. Meanwhile, shear fissures generate AEs with longer wavelengths, and the AE waveform has a longer rising time and lower frequency. Therefore, the ratio of rising time to amplitude of AE signals (RA; units: ms/V) can be used to study rock failure mechanisms. Higher RA values correspond to tensile fissures and lower RA values correspond to shear fissures. Figure 6 shows plots of sample stress and RA with compressional loading time for different types of sandstone.

As shown in Fig. 6, the RA values of the AEs of the sandstones are generally low during the compression, and only a small number of higher RA values occur at around the time of failure. This shows that shear failure is dominant in the sandstones, and only a few tensile failures occur near the peak stress under uniaxial compression. This can be attributed to the fact that, in the fissure closure stage, the original cracks inside the sample are compacted. This means that no fissures grow and converge, and the occurrence frequency of AEs is relatively low. After entering the elastic deformation stage, with increasing stress, the fissures inside the sample are completely closed and begin to sprout and propagate, and some cracks begin to appear. The above process is accompanied by a small number of AEs, and the RA values of these AEs are small, thus suggesting that shear fissures are the

Table 3 Mechanical properties of different types of sandstone

Sample	σ_c (MPa)	E_s (GPa)	μ	Sample	σ_t (MPa)	Sample	Angle (°)	C (MPa)	tan φ	φ (°)
A1-1-1	18.47	1.18	0.16	A1-2-1	3.13	A1-3-1	45	3.57	0.62	31.95
A1-1-2	50.85	2.18	0.26	A1-2-2	1.59	A1-3-2	55			
A1-1-3	34.34	1.80	0.32	A1-2-3	3.77	A1-3-3	65			
A2-1-1	33.25	1.26	0.22	A2-2-1	2.69	A3-1	45	3.71	0.67	33.74
A2-1-2	38.02	1.92	0.23	A2-2-2	3.72	A2-3-2	55			
A2-1-3	39.92	1.83	0.22	A2-2-3	4.44	A2-3-3	65			
A3-1-1	34.73	1.38	0.44	A3-2-1	3.34	A3-3-1	45	4.57	0.78	38.1
A3-1-2	41.12	2.19	0.26	A3-2-2	5.13	A3-3-2	55			
A3-1-3	37.34	1.92	0.28	A3-2-3	4.69	A3-3-3	65			
A4-1-1	24.47	1.18	0.19	A4-2-1	6.02	A4-3-1	45	6.32	0.61	31.25
A4-1-2	43.71	1.87	0.21	A4-2-2	5.49	A4-3-2	55			
A4-1-3	51.50	2.01	0.22	A4-2-3	5.73	A4-3-3	65			
A5-1-1	37.19	1.61	0.18	A5-2-1	5.11	A5-3-1	45	4.57	0.78	38.1
A5-1-2	45.03	1.97	0.16	A5-2-2	3.82	A5-3-2	55			
A5-1-3	58.34	1.97	0.19	A5-2-3	4.53	A5-3-3	65			
B1-1-1	28.83	1.42	0.16	B1-2-1	1.14	B1-3-1	45	6.84	0.56	29.44
B1-1-2	42.05	2.05	0.24	B1-2-2	3.66	B1-3-2	55			
B1-1-3	82.83	2.62	0.19	B1-2-3	3.59	B1-3-3	65			
B2-1-1	48.32	1.56	0.23	B2-2-1	2.81	B2-3-1	45	5.1	0.72	35.65
B2-1-2	28.48	1.84	0.16	B2-2-2	4.95	B2-3-2	55			
B2-1-3	72.50	2.42	0.23	B2-2-3	5.65	B2-3-3	65			
B3-1-1	41.20	1.28	0.21	B3-2-1	4.35	B3-3-1	45	3.08	0.69	34.79
B3-1-2	57.27	1.97	0.22	B3-2-2	4.32	B3-3-2	55			
B3-1-3	28.96	1.45	0.21	B3-2-3	4.20	B3-3-3	65			
B4-1-1	50.33	1.48	0.14	B4-2-1	4.99	B4-3-1	45	8.42	0.42	22.68
B4-1-2	41.27	1.91	0.12	B4-2-2	6.37	B4-3-2	55			
B4-1-3	73.38	2.48	0.15	B4-2-3	4.97	B4-3-3	65			
B5-1-1	55.32	1.56	0.20	B5-2-1	3.81	B5-3-1	45	7.4	0.14	7.9
B5-1-2	40.25	1.79	0.25	B5-2-2	3.87	B5-3-2	55			
B5-1-3	53.62	2.43	0.22	B5-2-3	5.15	B5-3-3	65			
B6-1-1	45.71	1.44	0.15	B6-2-1	1.81	B6-3-1	45	6.67	0.6	30.95
B6-1-2	74.78	2.25	0.20	B6-2-2	2.74	B6-3-2	55			
B6-1-3	74.95	2.25	0.19	B6-2-3	2.23	B6-3-3	65			
B7-1-1	27.15	1.28	0.26	B7-2-1	4.73	B7-3-1	45	7.5	0.55	28.87
B7-1-2	56.27	2.02	0.24	B7-2-2	4.35	B7-3-2	55			
B7-1-3	52.30	2.13	0.19	B7-2-3	3.84	B7-3-3	65			
B8-1-1	31.40	1.27	0.23	B8-2-1	1.13	B8-3-1	45	2.76	0.75	36.9
B8-1-2	26.81	1.79	0.26	B8-2-2	1.50	B8-3-2	55			
B8-1-3	56.27	2.02	0.24	B8-2-3	2.33	B8-3-3	65			
C1-1-1	29.86	1.44	0.26	C1-2-1	0.80	C1-3-1	45	3.06	0.66	33.56
C1-1-2	39.92	1.83	0.25	C1-2-2	2.61	C1-3-2	55			
C1-1-3	27.74	1.31	0.28	C1-2-3	0.83	C1-3-3	65			
C2-1-1	41.20	1.87	0.29	C2-2-1	8.22	C2-3-1	45	9.18	0.59	30.58
C2-1-2	61.55	1.87	0.29	C2-2-2	5.45	C2-3-2	55			
C2-1-3	29.15	1.79	0.26	C2-2-3	6.95	C2-3-3	65			
C3-1-1	63.45	1.49	0.26	C3-2-1	7.72	C3-3-1	45	7.87	0.63	32
C3-1-2	82.08	2.67	0.30	C3-2-2	5.62	C3-3-2	55			
C3-1-3	26.87	1.79	0.29	C3-2-3	8.23	C3-3-3	65			

σ_c, uniaxial compressive strength; E_s, modulus of elasticity; μ, Poisson's ratio; σ_t, tensile strength; *angle*, angle of the plate clamp, which is also the angle between the shear stress and the horizontal direction; C, cohesive force; φ, angle of internal friction
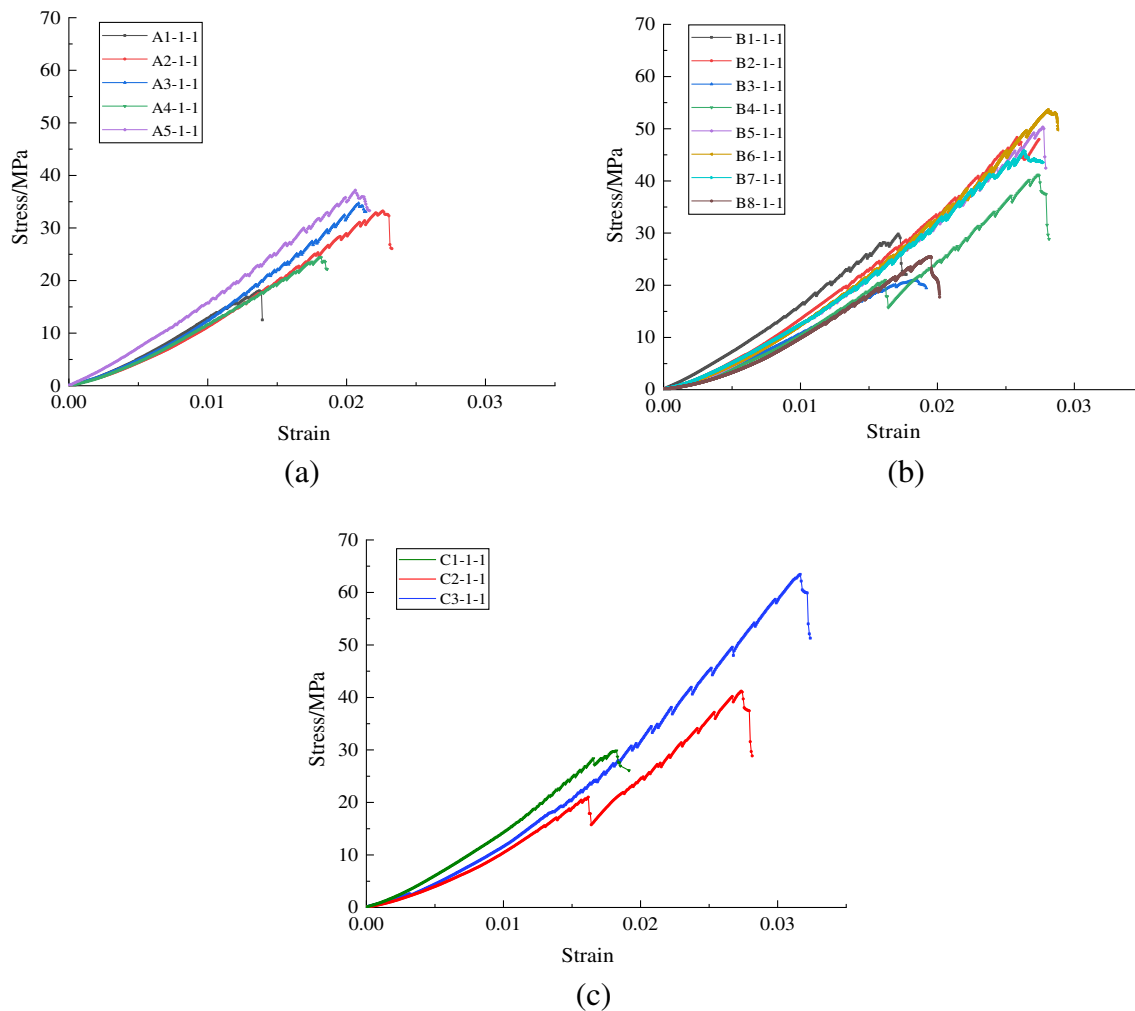
Fig. 5 Experimentally derived stress–strain curves for different types of sandstone under uniaxial compression. (**a**), (**b**), and (**c**) show the results for mine A (Jining No. 3 coal mine), mine B (Dongqu coal mine), and mine C (Xinqiao coal mine), respectively

dominant fissure type during this stage. In the inelastic deformation stage, internal fissures begin to propagate and converge around the main fissure. This leads to an increase in the number and amplitude of AE events, which results in the occurrence of many high RA values near the peak stress. This indicates that mostly tensile cracks are generated during the inelastic deformation stage.

As shown in Fig. 6, when the grain size of the sandstone increases, the number of high RA values observed in samples B3-1-1, B4-1-1, B1-1, and B7-1-1 near the peak stress significantly increases. This shows that the larger the grain size of the sandstone, the more tensile failures occur near the peak stress, with shear failure being the main failure mode in sandstone with smaller grain size near the peak stress. Additionally, the mineral content (e.g., quartz content) also affects the crack properties of the rock samples. The sandstone with a higher quartz content mainly suffers shear failure near the peak stress, while the sandstone with a lower quartz content mainly suffers tensile failure near the peak stress. For

example, in the coarse-grained lithic-debris greywacke (sample B7-1-1), whose quartz content is 2.3% lower than that of the fine-grained lithic-debris greywacke I (sample B3-1-1 shown in Table 2), a larger number of high RA values are observed near the peak stress.

Effect of mineral content on the mechanical characteristics of sandstone

Coal-bearing rocks are formed in the shallow crust (Meng et al. 2002). The diagenetic mechanism and disturbance of the external environment greatly influence the mineral composition and meso-structure of different rocks (Zhao et al. 2013). The main intrinsic factors which control the macro-mechanical properties of rock materials are mineral composition, particle size, and cementation type. Based on the micro- and meso-analysis of sandstone samples in the "Analysis of micro- and meso-characteristics of sandstone" section and the results of the stress–strain analysis in the "Mechanical

(a) Fine-grained lithic-debris greywacke

(b) Medium-fine lithic-debris greywacke

(c) Medium-grained lithic-debris sandstone
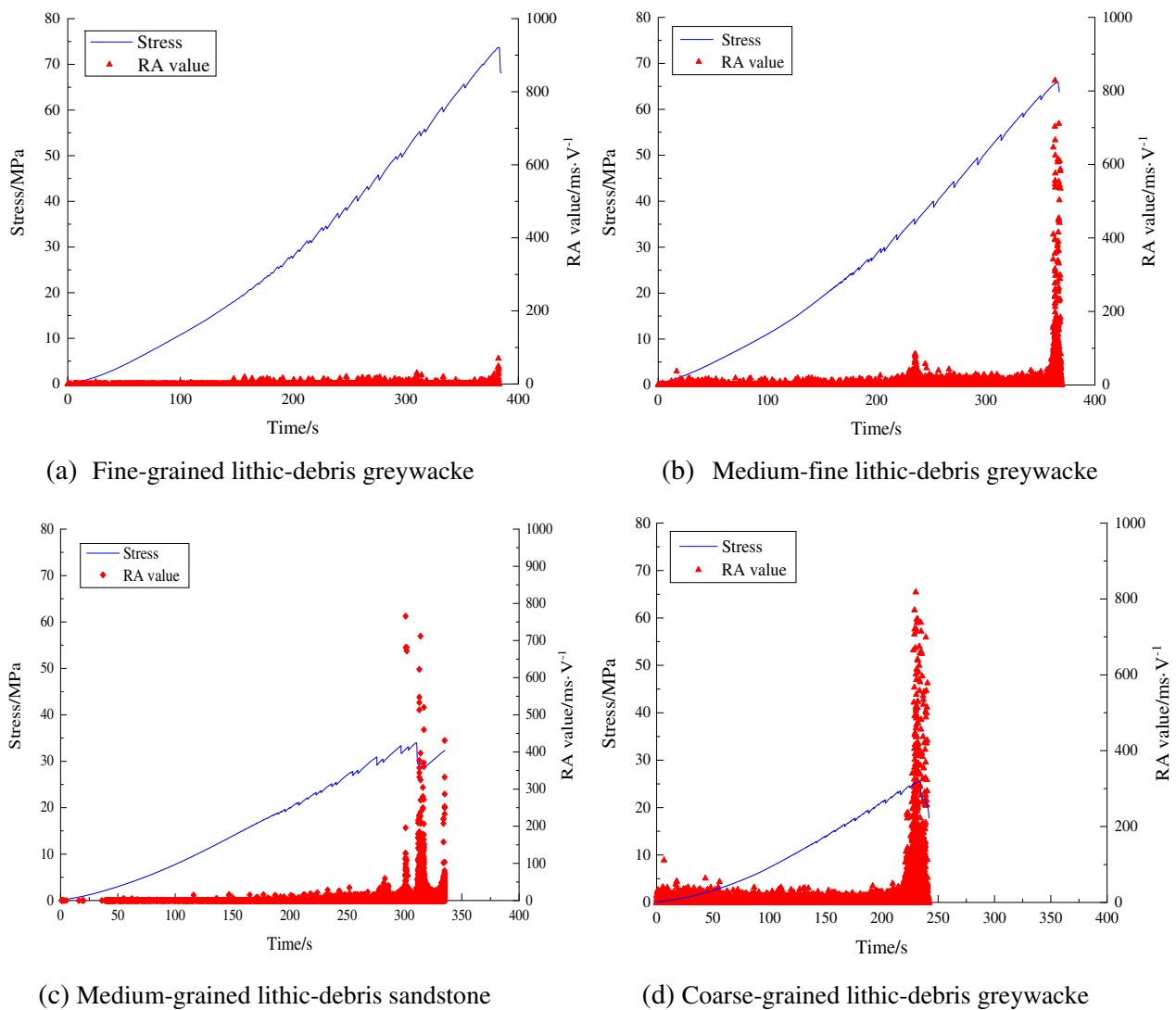
(d) Coarse-grained lithic-debris greywacke

Fig. 6 Stress and AE RA versus uniaxial compression loading time for various sandstone samples. (**a**) Sample B3-1-1. (**b**) Sample B4-1-1. (**c**) sample B2-1-1. (**d**) sample B7-1-1

properties and fissure characteristics of sandstones under uni-axial compression" section, in this section, we adopt a single-variable approach and select three rock samples which have a similar structure, cementation, particle contact, particle sup-port mode, and particle size, in order to study the effects of mineral content on the mechanical properties of rocks.

Figure 7 shows the experimentally derived relationships between the mineral contents and uniaxial compressive pa-rameters of rock samples. The analysis of microscopic and mesoscopic characteristics of sandstones in the "Analysis of micro- and meso-characteristics of sandstone" section shows that quartz mainly occurs as single crystals with a low poly-crystalline content, undeveloped cleavage, and a Mohs hard-ness of 7 (Sun 2002). The chemistry of quartz is very stable. Therefore, the presence of quartz can be assumed to increase

the uniaxial compressive strength and elastic modulus of the sandstone, as is suggested by Fig. 7a, b. This is consistent with the results of previous studies (Zhao et al. 2013). On the con-trary, with increasing plagioclase content, the uniaxial com-pressive strength and elastic modulus of the rock samples decrease, as shown in Fig. 7c, d. This can be mainly attributed to the development of cleavage in the plagioclase (as observed by microscopic observation) and the fact that the plagioclase is partly sericitized and lightly fractured. Plagioclase feldspar is an aluminosilicate mineral. Compared with quartz, feldspar has lower hardness and less stable chemical properties. Moreover, it is easily weathered into clay minerals under nat-ural conditions. Therefore, the presence of feldspar reduces the uniaxial compressive strength and elastic modulus of the sandstone.
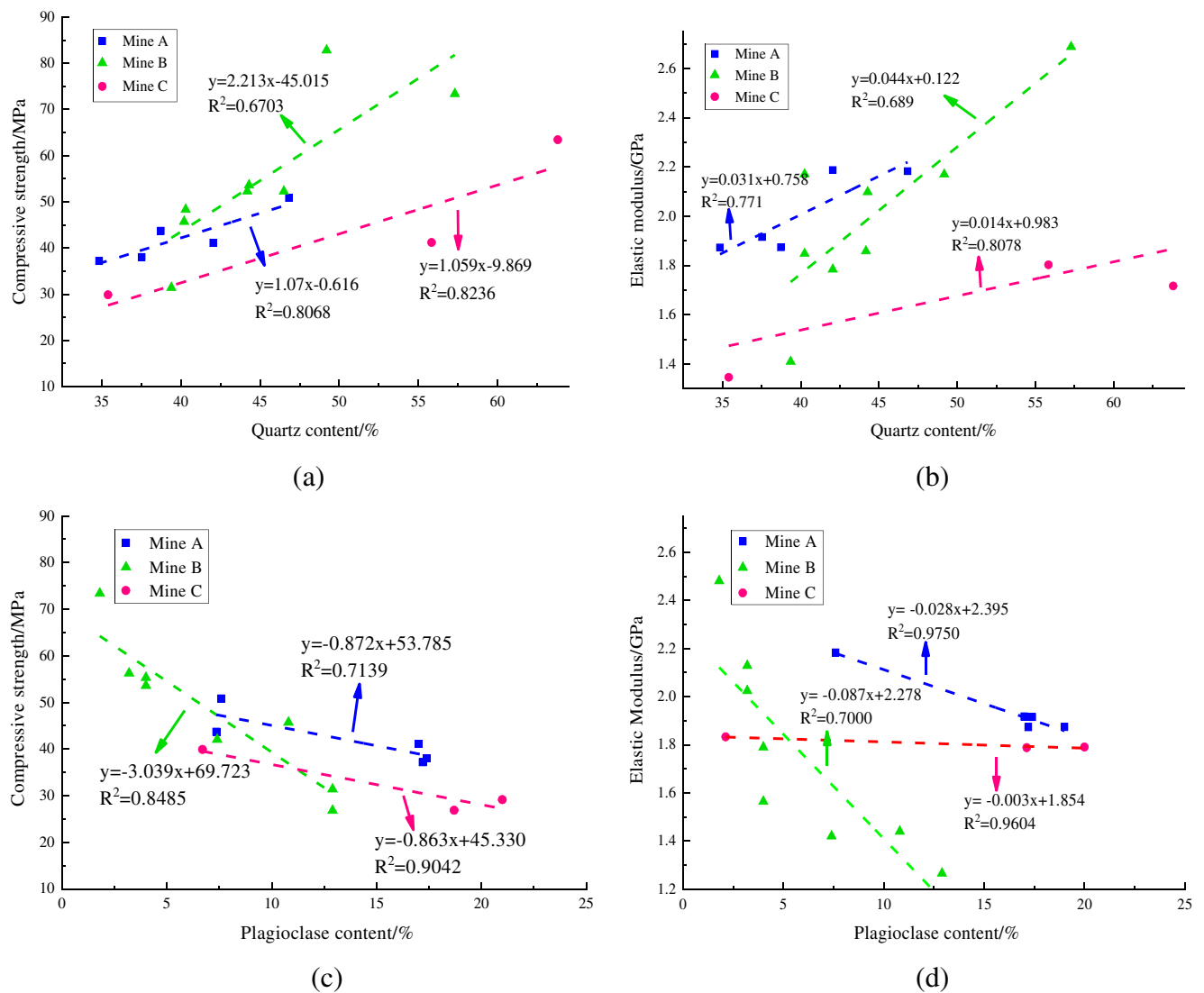
Fig. 7 Experimentally derived relationships between sample mineral content and uniaxial compression. Mine A represents Jining No. 3 coal mine, mine B represents Dongqu coal mine, and mine C represents Xinqiao coal mine

Figure 7 e and f show the effects of clay mineral contents on the mechanical properties of rock samples. From the figure, it can be seen that the uniaxial compressive strength and elastic modulus of sandstones are negatively correlated with clay mineral content. This can be attributed to the fact that the clay minerals are mainly kaolinite, illite, chlorite, etc., which have low hardness and unstable chemical properties, and therefore lead to the reduction of the rock's macroscopic compressive strength and elastic modulus. Previous researchers (Lindqvist et al. 2007) have come to the same conclusion. As shown in Table 4, kaolinite is the dominant clay mineral in all of the sandstones analyzed in this study. Kaolinite is chemically unstable. In sandstone samples with a higher kaolinite content, pores are larger and more abundant, the internal connection of the rock is low, and the rock compactness is low. Accordingly, such rocks will have weaker macro-mechanical properties, as

reflected in the reduction of compressive strength and elastic modulus shown in Fig. 7g, h.

By also considering the results shown in Table 3 and Fig. 8, it can be seen that the effect of mineral content on the tensile strength, cohesion, and internal friction angle of rock samples is similar to its effect on compressive strength. This further shows that mineral content is one of the controlling factors of rock micro- and macro-mechanical properties.

Effect of particle contact rate on the mechanical characteristics of sandstones

Based the analysis of the micro- and meso-characteristics of sandstones presented in the "Analysis of micro- and meso-characteristics of sandstone" section, the contact modes of particles can be divided into four types: non-contact, point
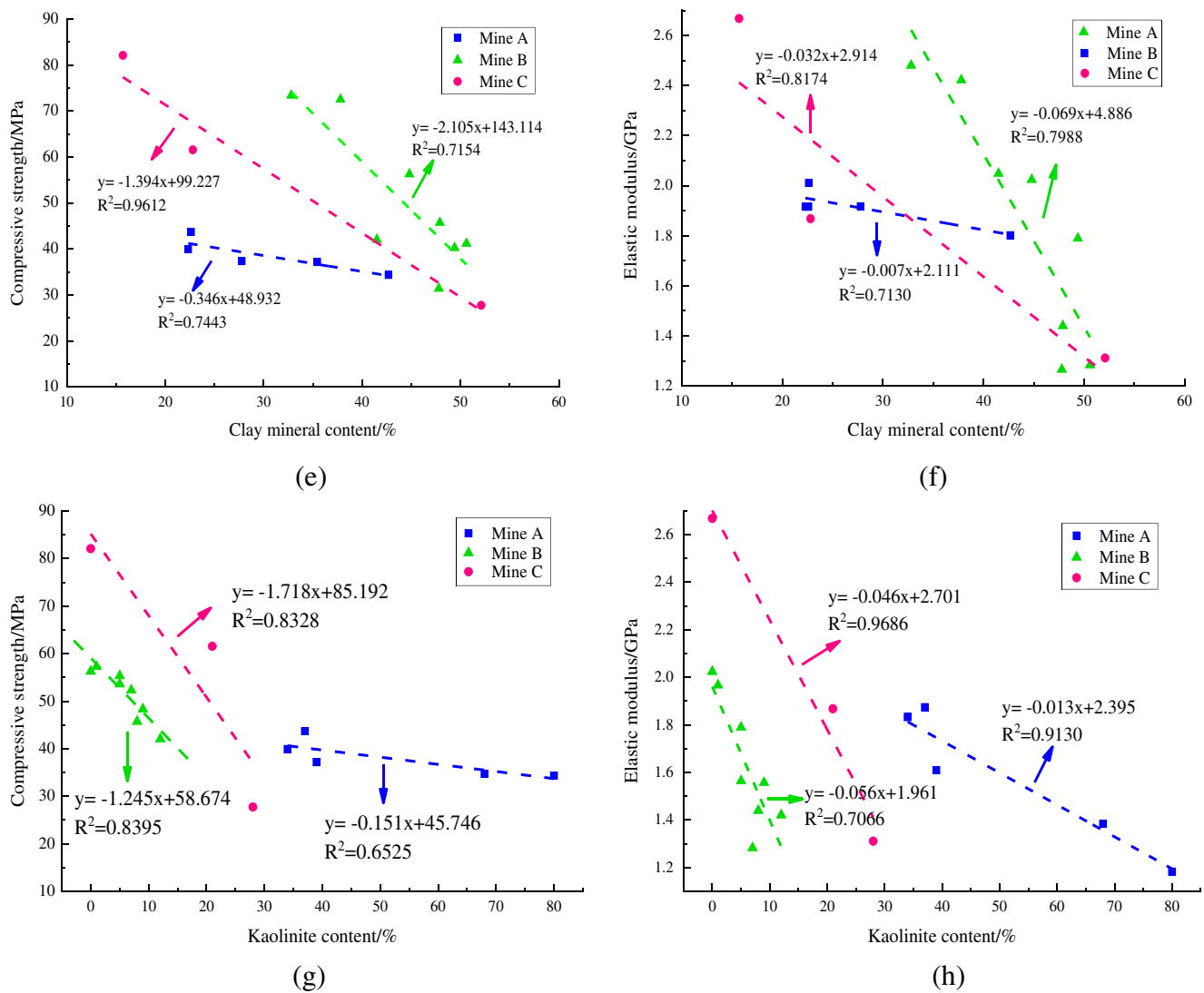
(e)

(f)

(g)

(h)

Fig. 7 (continued)

contact, line contact, and concave–convex contact. With increasing particle size, the contact mode of particles changes from concave–convex contact or line contact to point contact or non-contact, and the contact rate of particles decreases. Figure 9 shows the relationship between the particle contact style and the mechanical parameters of rock samples. From Fig. 9a, b, it can be seen that with increasing particle contact rate, the uniaxial compressive strength and elastic modulus of sandstones in mine B increase from 26.81 to 82.83 MPa and from 1.36 to 2.62 GPa, respectively. The values of the compressive strength and elastic modulus of mine A and mine C are relatively dispersed, but the overall trend is also increasing. That is, the mechanical properties of rock samples clearly increase with increasing particle contact rate. This is similar to the conclusions reached by earlier researchers (Přikryl 2001).

Figure 9 c and d show the relationships between particle contact degree and rock cohesion and internal friction angle.

With increasing particle contact rate, the cohesive force of sandstones in mine C increases from 3.06 to 9.18 MPa, and the tangent of internal friction angle increases from 0.59 to 0.66, respectively. Although the data of sandstones in mine A cannot be well fitted linearly, the overall trend is also increasing. The data of sandstones in mine B are relatively dispersed, which may be related to the degree of sample integrity. In a word, the cohesive force and tangent of internal friction angle of rock samples are positively correlated with the particle contact rate, that is, on the whole, the cohesive force and internal friction angle of the rock sample both increase with increasing particle contact rate. This is similar to the conclusions reached by earlier researchers (Zhao et al. 2013). This is mainly due to the fact that the larger the particle contact rate, the larger the number of particles per unit volume, the more compact the rock, and the greater the contact force between the particle units.

Table 4   Uniaxial compressive strength and cementation of different types of sandstone

Sample	σ_c(MPa)	E_s(MPa)	Cementation type	
			Cement content (vol.%)	Description
A1-1	18.47	1182.42	< 1	Mainly authigenic clay minerals and argillaceous cementation.
A2-1	38.02	1915.53	< 1	Carbonate content is very low, metasomatic feldspar.
A3-1	41.12	2187.60	< 1	Carbonate content is very low, metasomatic feldspar.
A4-1	24.47	1179.41	2	Carbonate content is very low, metasomatic feldspar.
A5-1	58.34	1965.71	2	Carbonate, ankerite, and siderite
B1-1	82.83	2618.39	25	Carbonates—mainly calcite, ankerite and siderite; iron after oxidation of siderite
B2-1	28.48	1841.78	1	A small amount of ankerite and siderite. Limonitization occurs along rhombic cleavage for locally idiomorphic-crystal ankerite.
B3-1	57.27	1966.84	5	Calcite is dominant; a small amount of rhombic idiomorphic crystalline dolomite; flash protrusion is obvious.
B4-1	50.33	1479.88	3	Calcite is dominant; a small amount of rhombic idiomorphic crystalline dolomite; flash protrusion is obvious.
B5-1	55.32	1564.32	3	Calcite is dominant; a small amount of rhombic idiomorphic crystalline dolomite; flash protrusion is obvious.
B6-1	74.95	2248.68	8	Siderite content is about 4%, with siderite occurring as micro- to fine-grained single crystals; aggregates are irregularly shaped blocks distributed in micro-sections; calcite content is about 3%.
B7-1	27.15	1282.19	2	Mainly authigenic clay minerals, occasionally rhombic crystalline dolomite.
B8-1	31.4	1265.70	2	Mainly authigenic clay minerals, occasionally rhombic crystalline
C1-1	27.74	1311.14	1	Mainly authigenic clay minerals, occasionally siderite
C2-1	29.15	1790.39	1	Mainly authigenic clay minerals, occasionally siderite
C3-1	26.87	1787.86	1	Mainly authigenic clay minerals, occasionally siderite

Analysis of the qualitative relationship between cementation type and uniaxial compressive strength

In rock debris, cementation includes cements or fissure fillings and the contact between cements and debris particles. Cementation is usually divided into argillaceous, calcareous, siliceous, and iron. Table 4 shows the uniaxial compressive strength and cementation type of different types of sandstone.

From Table 4, it can be seen that the higher the percentage of cement, the higher the compressive strength and elastic modulus of the rocks. This can be attributed to the fact that rock porosity reduces with increasing cementation. As shown
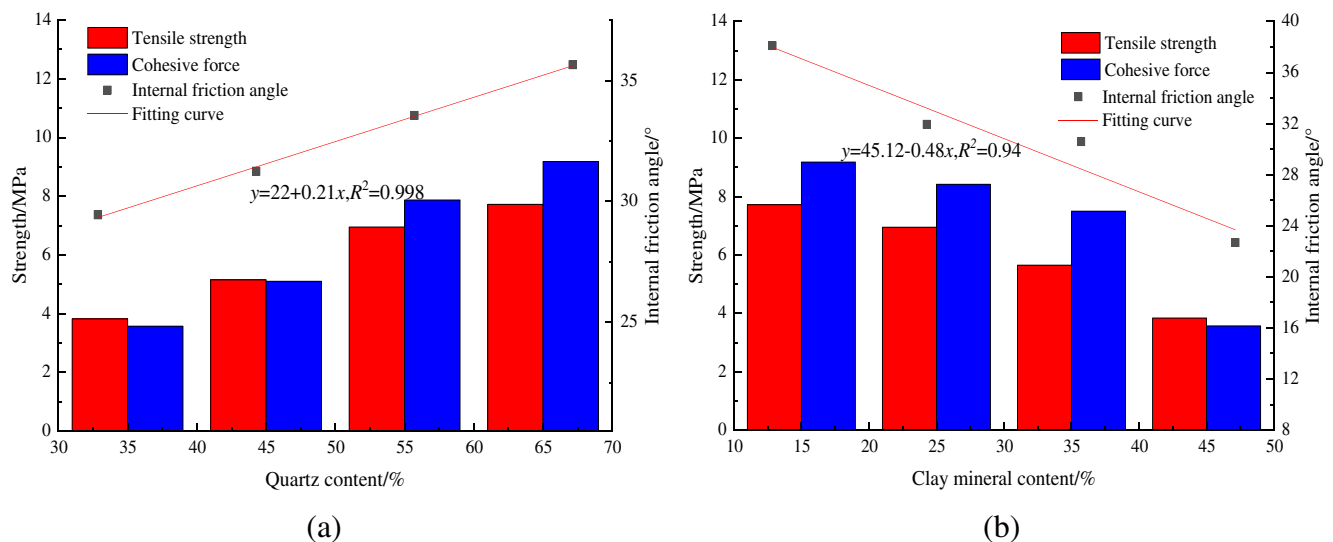

(a)   (b)

Fig. 8 Experimentally derived relationships between sample mineral content and tensile and shear parameters
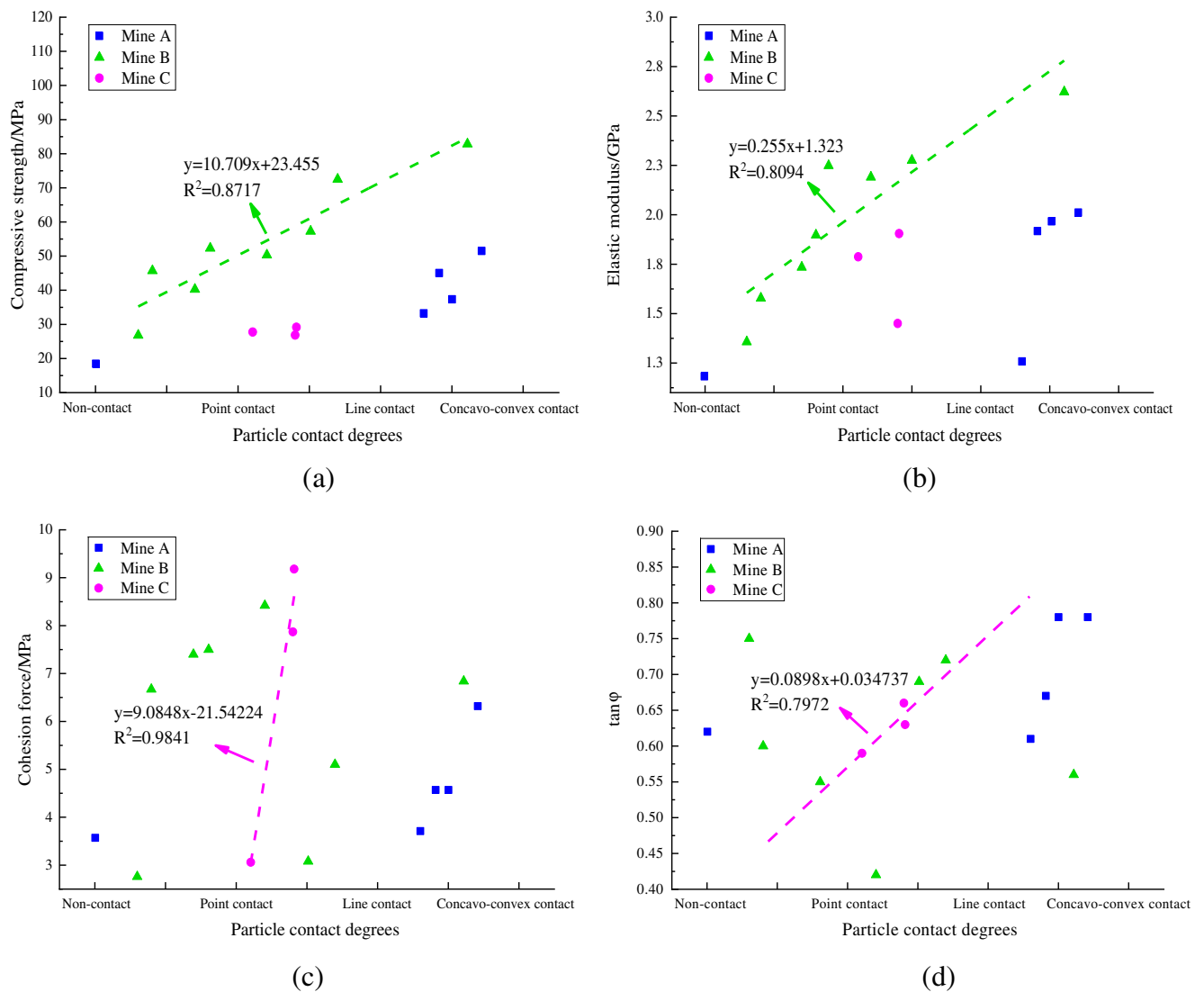
Fig. 9 Experimentally derived relationships between particle contact mode and the mechanical parameters of rock samples

in Table 4, the uniaxial compressive strengths of samples B3-1 and B6-1—which are cemented with carbonate and siderite, respectively—are 57.27 and 74.95 MPa, respectively, while the uniaxial compressive strength of sample C2-1, whose cement is mainly composed of clay minerals, is 29.15 MPa. This indicates that rocks which are cemented by carbonate and siderite are stronger than those which are cemented by clay minerals.

Evolution characteristics of sandstone damage

Strength damage model for sandstone specimens

Damage mechanics is generally used to study the relationship between the strength and deformation of rocks.

In this study, based on the randomness of the strength distribution of rock micro-elements, a quantitative relationship between damage variables and stress and strain is established for the rocks, and then a constitutive model for this relationship is established to simulate the damage to the rocks with increasing stress. Then, the simulation results of the established constitutive damage model were compared with the experimentally derived stress–strain relationships. In this section, the mechanical failure characteristics of different types of sandstone specimens under uniaxial compression are studied, and a piecewise-curve damage model based on cumulative AE counts is established. The piecewise-curve model considers that damage evolution always occurs before and after the peak strength is reached. The following equations were adopted to fit the stress–strain data (Xu 2007):

$$D = \begin{cases} a\left(\dfrac{\varepsilon}{\varepsilon_c}\right)^b & (0 \leq \varepsilon \leq \varepsilon_c) \\ 1 - \dfrac{c}{k\left(\dfrac{\varepsilon}{\varepsilon_c}\right)^d + \dfrac{\varepsilon}{\varepsilon_c}} & (\varepsilon_c < \varepsilon) \end{cases} \quad (1)$$

Where a, b, c, d, and k are material constants; $a + c = 1$; and d and k are determined by fitting the experimental data. In this paper, values of $d = 1.765$ and $k = 0.0021\sigma_c$ were taken, where σ_c represents the uniaxial compressive strength.

According to boundary conditions, $\sigma|_{\varepsilon=\varepsilon_c} = \sigma_c$, $\frac{d\sigma}{d\varepsilon}|_{\varepsilon=\varepsilon_c} = 0$ then

$$a = \frac{E\varepsilon_c - \sigma_c}{E\varepsilon_c} \quad (2)$$

$$b = \frac{\sigma_c}{E\varepsilon_c - \sigma_c} \quad (3)$$

$$c = \frac{\sigma_c}{E\varepsilon_c} \quad (4)$$

The stress–strain curve and damage evolution curve obtained using the piecewise-curve damage model are shown in Fig. 10. This model considers that there is damage evolution before and after the stress reaches the peak stress, which is indicated by dotted lines. It is close to the Mazars model (Li 2002), except that the phase before the peak of the σ-ε curve is not linear, and therefore more scientific.

The simulated damage evolution curve based on cumulative AE counts was fitted using the Origin software (OriginLab Corporation, Northampton, MA, USA), as shown in Fig. 11. Because the fitting process is relatively simple, and in order to reduce the length of the paper, only the damage curves of A2-1 and A3-1 are shown in the paper.

After fitting the damage evolution curve, the damage evolution equation was obtained using the following equation:

$$D = \frac{m}{1 + e^{-k(\varepsilon-n)}} \quad (5)$$

where k, m, and n are curve parameters obtained by fitting the damage curve.

Damage constitutive relation of sandstone under uniaxial compression

According to Lemaitre's strain equivalence hypothesis (Li 2002), in the one-dimensional case, the stress term $[\sigma]$ in the strain constitutive relation of intact materials can be replaced by the effective stress $[\sigma]'$ (Yu 2009). Therefore, the damage constitutive relation can be expressed as follows:

$$[\sigma] = [\sigma]'(1-D) = [H][\varepsilon](1-[D]) \quad (6)$$

where $[\sigma]$ is the stress matrix, $[\sigma]'$ is the effective stress matrix, $[H]$ is the material elastic matrix, $[\varepsilon]$ is the strain matrix, and

$[D]$ is the variable damage matrix.

Assuming that the damage distribution in the sandstone samples is isotropic, under loading, local micro-fissures will change the mechanical properties of the samples, and macro-fissures will not appear. From continuum damage-mechanics theory (Zhao 2002; Xie et al. 2004; Liu 2012), the constitutive stress–strain relation of the sandstone samples can be obtained as follows:

$$\sigma = [\sigma]'(1-D) = E\varepsilon(1-[D]) \quad (7)$$

Within the rock samples, there are many defects such as fissures, pores, and material interfaces. The sizes, shapes, and spatial distributions of these defects are random, and consequently the rock strength (which is closely related to these parameters) is also a random variable. Furthermore, a "size effect" exists in the rock samples. That is, with decreasing rock-sample size, the relative degree of nonlinearity of the rock's mechanical characteristics decreases. When the size of the rock sample decreases to a certain point, the mechanical properties of the rock sample show obvious elastic–brittle characteristics.

By introducing the damage variables which were determined from the fitting of the cumulative AE counts into Eq. (7), the one-dimensional elastic damage constitutive model for the sandstone based on the experimentally derived stress–strain curves can be obtained as follows:

$$\sigma = E\varepsilon\left(1 - \frac{m}{1 + e^{-k(\varepsilon-n)}}\right) \quad (8)$$

The simulated and experimentally derived stress–strain curves are shown in Fig. 12.

From the simulated and experimentally derived damage curves for the sandstone under uniaxial compression (Fig. 12), it can be seen that the established damage constitutive model is consistent with the experimental results. However, there are differences between the simulated and experimentally derived results. For example, for a few samples, the simulated stress is slightly larger than the experimentally derived stress. These differences may be due to the following:

1. For a given strain, the simulated peak stress is greater than the experimentally derived peak stress. This may be due to the fact that, during the initial deformation of the sandstone, micro-crack events are less energetic, and the amplitudes of the resulting AEs are too low to be detected by the AR, thus leading to a discrepancy between the measured and simulated number of AEs.
2. The measured acoustic emission signals are composed of (i) the p-wave and s-wave which are emitted by the acoustic emission source and (ii) the sum of a series of waves transmitted to the interface of the rock sample after the transformation of various waveforms. This can lead to

Fig. 10 The stress–strain curve (**a**) and damage evolution curve (**b**) obtained using the piecewise-curve damage model that was used in the present study (Xu 2007); σ, stress; σ_c, uniaxial compressive strength; ε, strain; ε_c, peak strain; D, damage variable

(a) (b)
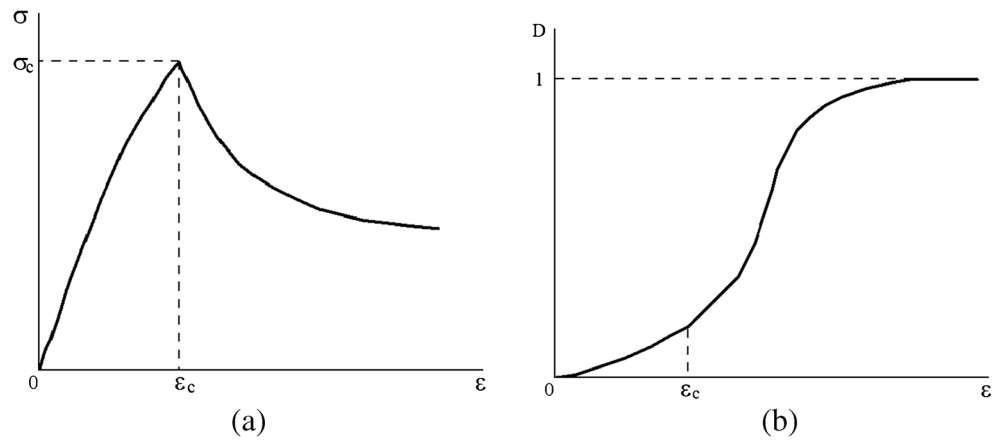
errors in the acoustic emission counts, which may explain the deviation between the theoretical curve and the experimental curve.

3. The deviation between the theoretical and experimental curves may be due to the selection of the initial parameters (e.g., d and k). Additionally, this deviation may have been exacerbated by the fact that, while the relationship between acoustic emission count and loading time was measured in the experiment, the theoretical calculation considered the relationship between acoustic emission count and strain.

Conclusion

Based on the research results, the following main conclusions are drawn:

1. Taking Jining No. 3 coal mine, Dongqu coal mine and Xinqiao coal mine as the research mines, it was

determined through the rock thin-film test that the sandstones studied can be divided into 16 types, including muddy, calcareous, fine-grained, medium-fine-grained, and medium-grained. Based on X-ray diffraction experiments, the mineral composition and microstructure characteristics of coal measures sandstone were studied, and we analyzed the grain characteristics, cementitious components, and cementation types of sandstone in different mining areas. The research results prove the rock structure and lithology information of these areas, and provide basic data for the application of in situ testing technology of coal and rock strength in these areas, which is conducive to the original parameter setting and range selection of related equipment.

2. Based on the physical and mechanical experiments, the mechanical properties such as σ_c, σ_t, C, and φ of the sandstone at the micro-scale and meso-scale were studied. The quartz content, cement content, and contact rate of large particles were found to be positively correlated with the mechanical strength of the sandstone, while the clay
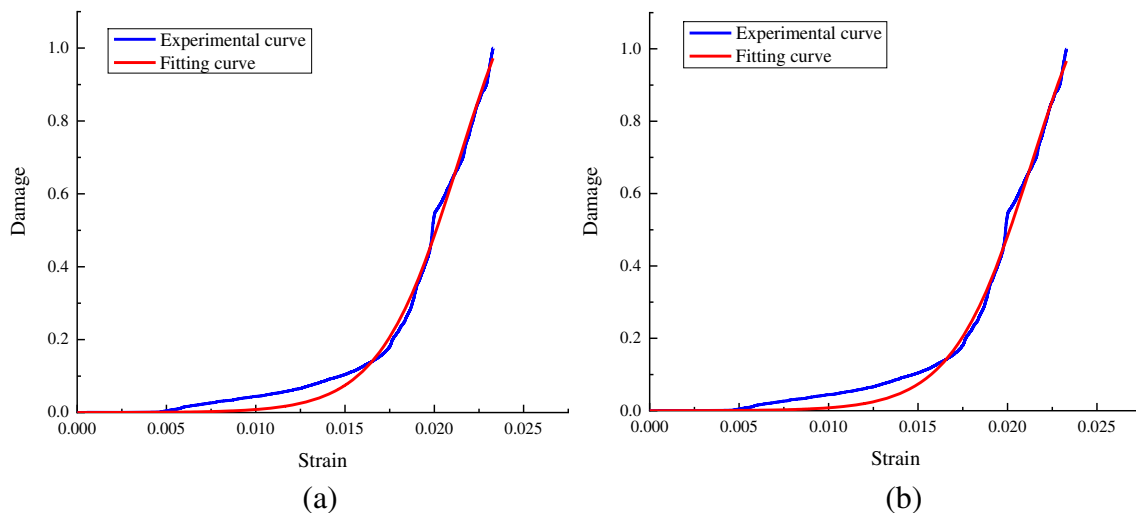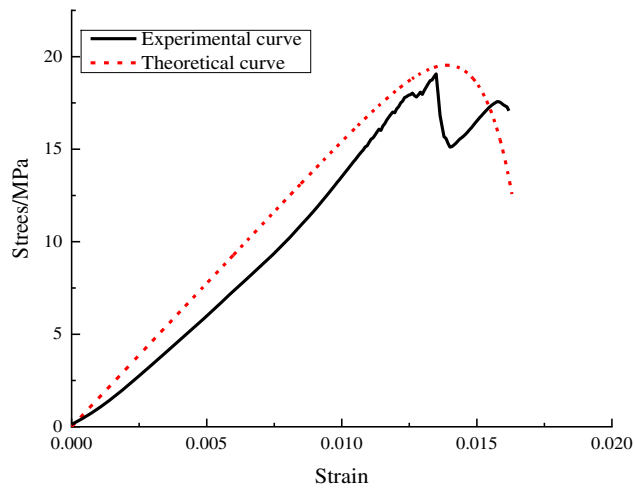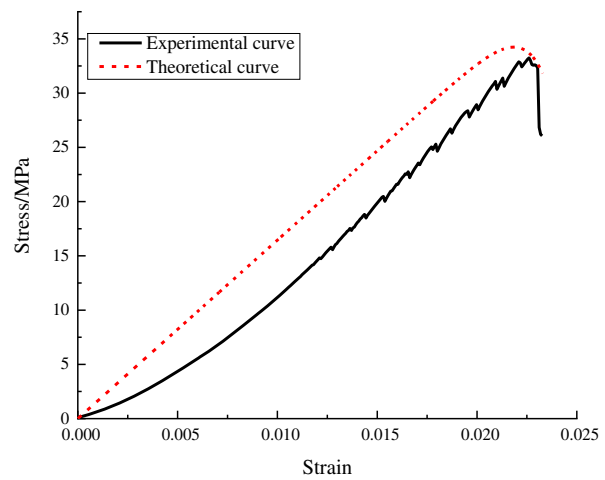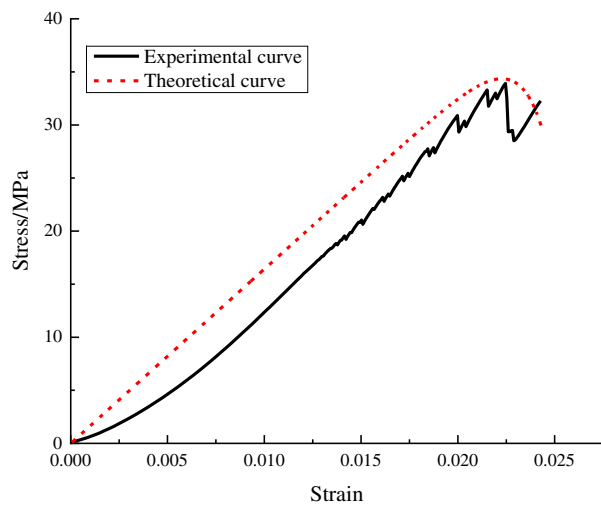

(a) (b)

Fig. 11 Comparison of the simulated and experimentally derived damage evolution curves for samples A2-1 and A3-1
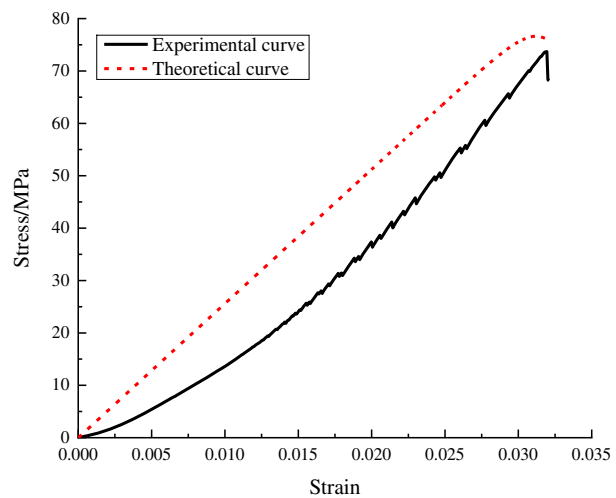
(a) Argillaceous fine-grained feldspar quartz greywacke

(b) Medium-fine lithic-debris feldspar sandstone

(c) Fine-grained lithic-debris greywacke

(d) Medium-fine lithic-debris greywacke

Fig. 12 Theoretically and experimentally derived stress–strain curves for sandstones under uniaxial compression. (**a**) sample A1-1-1. (**b**) sample A2-1-1. (**c**) sample B3-1-1. (**d**) sample B4-1-1

mineral content (especially the kaolinite content) was found to be negatively correlated with the mechanical strength of the sandstone. These research results complement and expand the related research on the influence of mineral composition on rock mechanical properties, and the subsequent researchers can further deepen the research on this basis, and explore the internal mechanism of the impact of mineral content on rock mechanical properties.

3. Fissure propagation in the sandstone was inferred using measurements of AEs. Under uniaxial compression, the RA value is generally at a low level, and only a small number of high RA values are generated when the rock sample is damaged, which means that the failure mode of sandstone is mainly shear failure. Additionally, the larger the particles, the lower the quartz content, the more high

RA values the rock produces near the peak stress, indicating that the more tensile failures occur.

4. Based on the cumulative AE counts combined with the existing research basis, a damage model for the sandstone under uniaxial compression was established, which can clearly show the specific process of rock failure. Taking the elastic modulus and strain as variables, the constitutive stress–strain relationship is derived. Based on this, the theoretical curve of uniaxial compression test is drawn, which can accurately reflect the test results and restore the actual situation. In practical application, this curve can be used to predict the damage degree of rocks with similar conditions to some extent.

Compliance with ethical standards

Conflict of interest   The authors declare that they have no conflict of interest.

References

Arbabi S, Sahimi M (1993) Mechanics of disordered solids. I Percolation on elastic networks with central forces. Phys Rev B 47(2):695–702

Bai CX, Liu Y, Wang D, Feng X, Liu C, Wang SY (2007) The application of Rayleigh wave testing techniques to geotechnical engineering. Prog Geophys 22(6):1959–1965

Barbero EJ, Greco F, Lonetti P (2005) Continuum damage-healing mechanics with application to self-healing composites. Int J Damage Mech 14(1):51–81

Charles F (2002) Geomechanics issues related to long-term isolation of nuclear waste. Cr Phys 3(7):961–974

Darabi MK, Al-Rub RKA, Little DN (2012) A continuum damage mechanics framework for modelling micro-damage healing. Int J Solids Struct 49(3–4):492–513

Ersoy A, Waller MD (1995) Textural characterisation of rocks. Eng Geol 39(3–4):123–136

Feng B (2012) Study on coal-accumulating characteristic of Shanxi formation and low Shihezi formation in Yongcheng Coalfield Henan province. Journal of Henan Polytechnic University (natural science) 31(02):177–181

Fonseka GU, Krajcinovic D (1981) The continuous damage theory of brittle materials, part II: uniaxial and plane research model. Int J Appl Mech 48(4):816–824

Grosse CU, Ohtsu M (2018) Acoustic emission testing. Spring Science & Business Media, Berlin Heidelberg

Homand F, Giraud A, Escoffier S, Koriche A, Hoxha D (2004) Permeability determination of a deep argillite in saturated and partially saturated conditions. Int J Heat Mass Transf 47(14–16):3517–3531

Hudson J A, Harrison J P (2009) Engineering rock mechanics (vol. 1): an introduction to the principles. Science Press, Beijing

Johansson E (2011) Technological properties of rock aggregates. Lulea tekniska universitet, Dissertation

Kang HP, Lin J (2001) New development in geomechanics measurement and test technology of mine roadway surrounding rock. Coal Science and Technology 29(7):27–30

Kang HP, Wang JH (2007) Rock bolting theory and complete technology for coal roadways. China Coal Industry Publishing House, Beijing

Lemaitre J (1996) A course on damage mechanics II. Springer, Heidelberg

Li ZX (2002) Damage mechanics and application. Science Press, Beijing

Li L, Michel A (2003) A general relationship between porosity and uniaxial strength of engineering materials. Can J Civ Eng 30(4):644–658

Lindqvist JE, Akesson U, Malaga K (2007) Microstructure and functional properties of rock materials. Mater Charact 58(11–12):1183–1188

Liu YK (2012) Damage evolution and rheological behavior of deep rock mass under water-rock interaction. Central South University, Dissertation

Ma WX, Chen ZJ, Wang ZL (2012) In-situ rapid measuring technology and application of coal and rock strength. Coal Science and Technology 40(2):22–24

Meng ZP, Su YH (2006) Physical theory and method of sedimentary rocks. Science Press, Beijing

Meng ZP, Peng SP, Qu HL (2000) The relationship between composition and texture of sedimentary rock and its mechanical properties in the roof and floor. Chin J Rock Mech Eng 19(2):136–139

Meng ZP, Peng SP, Fu JT (2002) Discussion on controlling factors of rock mechanical properties of coal-bearing rock series. Chin J Rock Mech Eng 21(1):102–106

Ministry of Land and Resources of the PRC (2015) Regulation for testing the physical and mechanical properties of rock. Standards Press of China, Beijing (in Chinese)

Muralha J, Grasselli G, Tatone B, Blümel M, Chryssanthakis P, Yujing J (2014) ISRM suggested method for laboratory determination of the shear strength of rock joints: revised version. Rock Mech Rock Eng 47(1):291–302

Peng BX, Liu YJ, Wang XH (2007) Application of the combined sound wave velocity-pressurization test method to soft rock in red layers. Rock Soil Mech 28(Supp):914–918

Přikryl R (2001) Some microstructural aspects of strength variation in rocks. Int J Rock Mech Min Sci 38(5):671–682

RäIsäNen M (2004) Relationships between texture and mechanical properties of hybrid rocks from the Jaala–Iitti complex, south eastern Finland. Eng Geol 74(3–4):197–211

Sahimi M, Arbabi S (1993) Mechanics of disordered solids. II Percolation on elastic networks with bond-bending forces. Phys Rev B 47(2): 703–712

Song MC, Jiao XM, Zhang CJ et al (2016a) Stratigraphic sequence and formation environment of Jining Group in Shandong Province. J Stratigr 40(01):26–40

Song MC, Jiao XM, Zhang CJ et al (2016b) An analysis of formation age of Jining Group in Shandong Province. Geol China 43(03):829–842

Su C (2016) Study on the sequence stratigraphy and the gas characteristics of Taiyuan formation in Gujiao mine area. China University of Mining and Technology, Dissertation

Sun PD (2002) Mohs hardness and scratch. Heat Treatment 17(4):16–16

Thury M, Bossart P (1999) The Mont Terri rock laboratory, a new international research project in a Mesozoic shale formation, in Switzerland. Eng Geol 52(3–4):347–359

Wang K, Yu QX (1998) Study on determination of coal mass strength by boring method. J China Coal Soc 23(6):601–605

Xie HP, Peng RD, Yan Y (2004) Analysis of energy dissipation during rock deformation and failure. Chin J Rock Mech Eng 23(21):3565–3570

Xu K (2007) The research on damages and distorts of rock-concrete. Xihua University, Dissertation

Xue GQ (2012) Analysis of geological characteristics of Yongcheng Coal mine field. Industry Technology 10:72

Yao QL, Li XH, Zhu L, Yan K, Yang P, Xia Z, Wang WT, Li DW (2019) Development and application of in-situ testing system for geomechanical parameters of coal and rock mass. J China Univ Min Technol 48(6):1169–1176

Yao QL, Tang CJ, Liu ZC (2020) Discussion on coal and water co-mining in ecologically fragile mining areas in western China. Coal Science and Technology http://kns.cnki.net/kcms/detail/11.2402. TD.20200215.2005.008.html

Yu HY (2009) Research and application on elastoplastic damage constitutive model for concrete based on ideally undamaged state. Chongqing University, Dissertation

Zhang PF (1990) Sedimentary petrology. Coal Industry Press, Beijing

Zhao X (2002) Damage mechanics and its application. Science Press Beijing

Zhao MJ, Wu DL (2009) The ultrasonic identification of rock mass classification and rock mass strength prediction. Chin J Rock Mech Eng 19(1):89–92

Zhao B, Wang ZY, Wu JP (2013) Relation between mineralogical composition and microstructure to the mechanical properties of rock materials. Coal Geology & Exploration 41(03):59–64

Zhou R, Yao YB, Liu DM et al (2017) Gas potential distribution and controlling factor of coal reservoir inTaiyuan Xishan Coalfield. Coal Science and Technology 45(02):122–129